

Dynamical Heterogeneity in Shear-Jammed Granular Systems

Yiqiu Zhao^{1,2,*}, Jonathan Barés^{3,**}, Hu Zheng^{4,5,***}, and Joshua E. S. Socolar^{1,****}

¹Department of Physics, Duke University, Durham, North Carolina 27708, USA

²Department of Physics, The Hong Kong University of Science and Technology, Hong Kong SAR, China

³Laboratoire de Mécanique et Génie Civil, Université de Montpellier, CNRS, Montpellier 34090, France

⁴Department of Geotechnical Engineering, College of Civil Engineering, Tongji University, Shanghai, China

⁵State Key Laboratory of Disaster Reduction in Civil Engineering, Tongji University, Shanghai, China

Abstract. Granular suspensions can jam into solids under shear at densities below the isotropic jamming density. At sufficiently large shear stress, these shear-jammed structures undergo plastic flow through small deformations of the particles, contact breaking or slipping, and associated particle rearrangements. Although the shear jamming phenomenon has been extensively studied in recent decades, little is known about how shear-jammed states evolve under steady shear. In this work, we report on systematic experiments on the evolution of a shear-jammed system using a recently developed multi-ring Couette shear device. This device imposes a linear shear profile on a layer of photoelastic discs, mimicking a two-dimensional suspension with a small Stokes number. We find that the displacements of the particles exhibit strong spatio-temporal correlations within the range of packing fractions where shear jamming occurs. The particle dynamics are quantified using the four-point susceptibility, which grows significantly as the packing fraction approaches the isotropic jamming point from below.

1 Introduction

Granular materials consist of large collections of non-Brownian particles that interact through simple repulsive contact forces. A characteristic behavior of granular materials is the jamming transition, where particles transition from a state with fluid-like properties to one with solid-like properties [1]. Over the past several decades, it has been established that this transition can be triggered not only by compression but also by shear [2, 3]. Shear-induced jamming strongly influences the rheology and mechanics of multiphase materials with a granular phase embedded in an incompressible medium, such as granular suspensions [4, 5] and soft compounds [6]. Although the mechanisms underlying the shear jamming transition have been extensively studied [7–9], the evolution of a shear-jammed particle network under continuous shearing remains less explored.

Photoelasticimetry is a widely used technique for studying shear jamming [3, 10]. This method enables the measurement of both particle displacements and contact forces in semi-2D granular systems composed of a layer of photoelastic particles. To investigate continuous shearing, earlier studies employed devices such as Couette shear cells, which impose shear from the boundaries [11]. However, boundary-driven shear cells pose challenges for probing shear jamming in dilute systems. To address this limi-

tation, a multi-slat shear device [12] and a multi-ring Couette shear device [13] were recently developed, both of which impose uniform shear profiles. The multi-ring Couette shear system, in particular, allows the investigation of shear-jammed states under continuous shear [14]. Although a shear jamming phase diagram has been mapped using this setup (Fig. 1a), the features of the steady states have not yet been systematically examined. Here, we present a study of the fluctuations in particle displacements about the average shear for shear-jammed packings of photoelastic disks.

2 Experiment

Our model granular system consists of bidisperse photoelastic discs. The radii of the large and small discs are $R_b = 7.95$ mm and $R_s = 6.35$ mm, respectively. The number ratio, ν , between the large and small particles is fixed at 1:3 for all experiments. The maximum static friction coefficient between two particles is $\mu \approx 0.9$, and the Young's modulus of the particles is approximately 6 MPa. The discs were cut from a polyurethane sheet using water jets, which produced rough boundaries on the discs (Fig. 1(b)) and, consequently, a large μ . The particles were sheared using a recently developed Couette shear device [13, 14] in which the particles rest on 21 concentric rings that rotated collectively to generate a linear shear profile (Fig. 1c and Supplementary Video 1). Shear was applied in a step-wise manner, with the granular system allowed to relax between consecutive steps. For each shear step, the tangential displacement $u_{t,\text{ring}}$ of a ring with radius r was set

*e-mail: yiqiuzhao@ust.hk

**e-mail: jonathan.bares@umontpellier.fr

***e-mail: zhenghu@tongji.edu.cn;

****e-mail: socolar@duke.edu

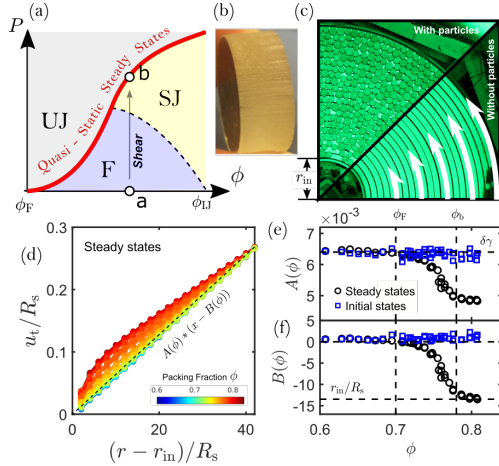


Figure 1. Probing the steady states in the shear jamming regime using the multi-ring Couette shear apparatus. (a) Shear jamming phase diagram (adapted from Ref. [14]). (b) A picture showing the rough lateral surface of a disc resultant from water cutting. (c) Multi-ring Couette shear apparatus imaged with and without particles. The setup contains 21 concentric rings that rotate collectively to impose a linear shear profile, as sketched by the white arrows. (d) Averaged tangential displacement of the particles per shear step (u_t) in the steady state plotted against the radial distance to the inner boundary ($r - r_{in}$). Both quantities are plotted relatively to the radius of the small discs R_s . The color of each curve represents the packing fraction ϕ of the corresponding experiment. For each curve, we fit data with $(r - r_{in})/R_s > 10$ to a linear function $y = A(x - B)$. The dashed black line plots one example best-fit result for $\phi = 0.63$. (e) The best-fit parameter A plotted as functions of ϕ for both the initial states and the steady states. (f) The best-fit parameter B plotted as functions of ϕ for both the initial and the steady states.

to $u_{t,ring} = \delta\gamma(r - r_{in})$, where $r_{in} = 8.7$ cm is the radius of the inner boundary, and $\delta\gamma$ is the imposed shear strain. The cumulative shear strain $\gamma \equiv \delta\gamma \times N_{step}$, where N_{step} is the total number of shear steps and $\delta\gamma = 0.0064$. Previous studies have confirmed that this method of imposing a linear shear profile does not produce any measurable layering in the radial distribution of disk centers [13].

We conducted experiments on granular systems with packing fractions, ϕ , ranging from 0.56 to 0.82. The packing fraction was varied by changing the number of particles from 1,447 to 2,101, keeping the number ratio $N_b/N_s = 3$. For each experiment, an unjammed configuration was prepared with the chosen ϕ . The boundaries and rings of the Couette device were then rotated so as to apply quasi-static shear to drive the system into the steady state. This process was illustrated as the transition from state a to state b in the phase diagram shown in Fig.1a. The system experienced a shear jamming transition before reaching the steady state [14]. In this study, we focus on the steady states.

3 Results

Averaged steady-state flow profile – The average quasi-static flow profile in the steady states depends on the packing fraction, ϕ . Figure 1d shows the radial distribution of

the tangential displacement of the particles, u_t , averaged over time in the steady-state regime for different values of ϕ . To quantify the ϕ -dependence, we fit the $u_t(r)$ data for each ϕ in the region $(r - r_{in})/R_s \geq 10$ to a linear function of the form $y = A(x - B)$, where A and B are fitting parameters. As shown in Figs.1e-f, for $\phi < \phi_F$, the fit parameters are $A \approx \delta\gamma$ and $B \approx 0$, indicating that the particles follow the imposed linear velocity profile. We note that $\phi_F \approx 0.7$ corresponds to the minimum packing fraction required to observe fragile states with non-zero pressure induced by shearing [14]. For $\phi > \phi_F$, both A and B decrease until they reach a plateau above $\phi_b \approx 0.78$. In this regime, $B \approx -r_{in}/R_s$, which implies $u_t = Ar$. This relationship describes a rigid body rotation, meaning the system consists of a rigidly rotating body in the region $(r - r_{in})/R_s > 10$ and a shear band at smaller r . In contrast to the steady-state profile, which exhibits a strong dependence on the packing fraction, the displacement profile of the initial state always follows the imposed linear velocity profile (Figs. 1 e-f).

Fluctuations in the flow – Now we consider the deviations of individual particle trajectories from the mean flow profile. Let $\mathbf{r}_i(\gamma)$ be the position of the i th particle at strain γ ; let $\mathbf{u}_i(\gamma_1, \gamma_2) = \mathbf{r}_i(\gamma_2) - \mathbf{r}_i(\gamma_1)$; and let $\mathbf{r}'_i(\gamma_1, \gamma_2)$ be the position that particle i would have at strain γ_2 if it followed the mean flow, which simply rotates its position by the angle associated with the change from γ_1 to γ_2 . We then define the deviated displacement to be

$$\delta\mathbf{u}_i(\gamma_1, \gamma_2) = \mathbf{r}_i(\gamma_2) - \mathbf{r}'_i(\gamma_1, \gamma_2). \quad (1)$$

Figures 2b-c show the real displacements, \mathbf{u}_i , and the deviated displacements, $\delta\mathbf{u}_i$, for a representative system with $\phi = 0.748$, measured between $\gamma_1 = 5.22$ and $\gamma_2 = 5.42$. The deviated displacements are spatially heterogeneous and form collective patterns.

The self-overlap parameter – To quantify the heterogeneous deviated particle displacements, we calculate the self-overlap parameter Q_s defined as [15]

$$Q_s(l, \Delta\gamma) = \langle \hat{Q}_s(l, \gamma, \Delta\gamma) \rangle = \left\langle \frac{1}{N} \sum_{i=1}^N H(l - |\delta\mathbf{u}_i(\gamma, \gamma + \Delta\gamma)|) \right\rangle, \quad (2)$$

where the average $\langle \cdot \rangle$ means averaging over different γ in the steady regime, $H(x)$ is the Heaviside step function, and l is a specified length. $Q_s(l, \Delta\gamma)$ measures the fraction of the grains that remains within a length l from their expected positions from the mean flow profile during a given strain interval $\Delta\gamma$. Figure 3a plots Q_s for an experiment with $\phi = 0.786$ using various l . Q_s decreases monotonically with $\Delta\gamma$, meaning that the particles tend to keep moving away from their expected positions from the mean flow profile.

Dynamical heterogeneity – We then calculate the four-point susceptibility χ_4 defined as

$$\chi_4(l, \Delta\gamma) = N \left(\langle \hat{Q}_s(l, \gamma, \Delta\gamma)^2 \rangle - \langle \hat{Q}_s(l, \gamma, \Delta\gamma) \rangle^2 \right). \quad (3)$$

For a given length scale l and a strain interval $\Delta\gamma$, χ_4/N measures the variance of $\hat{Q}_s(l, \Delta\gamma)$ starting from different γ . One can derive that χ_4 is the volume integral of a spatial correlation function [16–19]. Figure 3b plots χ_4 for

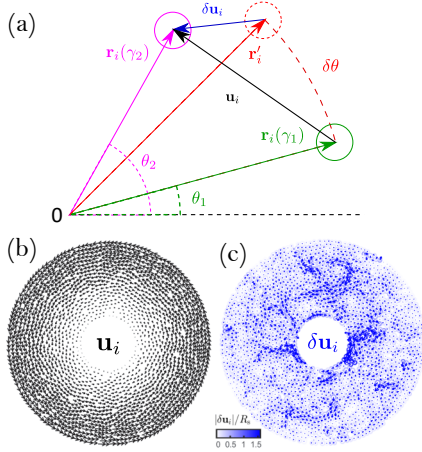


Figure 2. Quantifying the deviated particle displacement $\delta \mathbf{u}_i$ in the steady states. (a) Definition of deviated displacement, $\delta \mathbf{u}_i$. (b) Real displacements for each particle, $\mathbf{u}_i = \mathbf{r}_i(\gamma_2) - \mathbf{r}_i(\gamma_1)$, for an example run with $\phi = 0.748$ between $\gamma_1 = 5.22$ and $\gamma_2 = 5.42$. The length of the arrows is half of the magnitude of \mathbf{u}_i . (c) Deviated particle displacements $\delta \mathbf{u}_i$. The length of the arrows is set to be 3 times the magnitude of $\delta \mathbf{u}_i$ for better visualization. The boundaries of the discs are also plotted, and the color denotes the magnitude of $\delta \mathbf{u}_i$ following the color bar.

the same system as in Fig. 3a with various l . The qualitative features of $\chi_4(l, \Delta\gamma)$ in our steadily sheared granular system are similar to those obtained from cyclically sheared [16] and cyclically compressed [15, 20] granular systems: For each l , χ_4 shows a peak at some intermediate strain interval $\Delta\gamma^*$, meaning that the dynamics is most heterogeneous at this strain scale. As l increases, the peak strain $\Delta\gamma^*$ also shifts to larger values, demonstrating a growing length scale for the particle dynamics under increasing strain intervals. We denote the maximum value of χ_4 over all l and $\Delta\gamma$ as χ_4^\dagger , which corresponds to $l = l^\dagger$ and $\Delta\gamma = \Delta\gamma^\dagger$. For the $\phi = 0.786$ experiment shown in Fig. 3, $l^\dagger \approx 0.1R_s$ and $\Delta\gamma^\dagger \approx 0.3$. Consistently, previous experiments on cyclically compressed granular materials found that l^\dagger is approximately one-tenth of the particle radius [15]. To demonstrate the effect of $\Delta\gamma$, we plot the spatial distribution of the particles with $|\delta \mathbf{u}_i| > l^\dagger$ for three different $\Delta\gamma = 0.03, 0.30, \text{ and } 1.00$ in Fig. 3c-h. For each $\Delta\gamma$, we plot the distribution for two start strains $\gamma = 2.78$ and 3.74 . The susceptibility χ_4 peaks at $\Delta\gamma \approx 0.30$ means that the deviated displacements fluctuate most among different choices of γ . Indeed, qualitatively, the spatial patterns of the particles with large $\delta \mathbf{u}_i$ vary significantly in panels (e-f) of Fig. 3, but do not change much for panels (c-d) and (g-h).

Density dependence – Figure 4a shows the largest four-point susceptibility χ_4^\dagger as a function of the packing fraction ϕ . For $\phi < \phi_F \approx 0.7$, $\chi_4^\dagger \approx 1$ and is not sensitive to ϕ . χ_4^\dagger grows with ϕ when $\phi > \phi_F$. We note that ϕ_F marks the emergence of the force networks in the steady states (Fig. 4b-g). Thus, our results indicate that the force chains contribute to the heterogeneous dynamics of sheared granular materials.

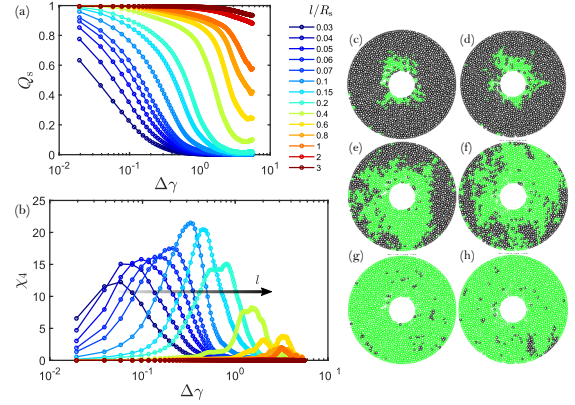


Figure 3. Dynamical heterogeneity in an experiment with $\phi = 0.786$. (a) The self-overlap parameter $Q_s(l, \Delta\gamma)$ against the strain interval $\Delta\gamma$ for different length scale l . (b) The four-point susceptibility χ_4 against the strain interval $\Delta\gamma$ for different length scale l . The legend applies for both (a) and (b) panels. (c-h) Spatial distribution of the particles with $|\delta \mathbf{u}_i| > l = 0.1R_s$ (green circles). For each panel, $|\delta \mathbf{u}_i|$ are calculated for a start strain γ and a strain interval $\Delta\gamma$. From (c) to (h), the parameters $(\gamma, \Delta\gamma)$ are (2.78, 0.03), (3.74, 0.03), (2.78, 0.30), (3.74, 0.30), (2.78, 1.00), and (3.74, 1.00).

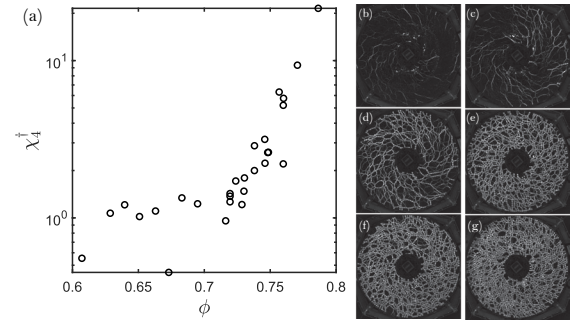


Figure 4. Dependence of dynamical heterogeneity on packing fraction. (a) The maximum χ_4 for each experiment, χ_4^\dagger , plotted against the packing fraction ϕ . The values plotted were calculated for experiments in which the collected data allowed for clear identification χ_4^\dagger . For $\phi > 0.776$, the data did not include applied shear strains large enough to show the maximum χ_4 values at large l . (b-g) Snapshots of the steady-state force networks. Each image was taken from experiments with varying packing fractions $\phi = 0.695$ (b), 0.716 (c), 0.738 (d), 0.757 (e), 0.776 (f), 0.798 (g). The images were captured using a polariscope, where stressed discs appear bright.

4 Conclusion

In this study, we examined the deviated particle displacements in continuously sheared granular materials within the shear jamming regime. We found that these deviated displacements exhibit heterogeneous spatial distributions. To quantify this dynamical heterogeneity, we calculated the four-point susceptibility, χ_4 . A detailed analysis of an experiment with $\phi = 0.786$ revealed that χ_4 peaks with a characteristic length, $l^\dagger \approx 0.1R_s$, and a strain interval, $\Delta\gamma^\dagger \approx 0.3$. Additionally, we investigated the density dependence of the largest χ_4 , denoted as χ_4^\dagger , and observed

that χ_4^\dagger increases with ϕ for $\phi > \phi_F \approx 0.7$, which is the smallest packing fraction at which force chains are detected [14]. These results suggest that the formation of force networks induced by shear jamming enhances the heterogeneous dynamics of deviated particle displacements in the steady states.

Previous studies have investigated dynamical heterogeneity in granular materials under cyclic shear [16, 21] or compression [15], but not under continuous shear. In the shear jamming regime, strong force networks emerge in the steady states (Fig.4b-g) but may disappear under cyclic shear depending on the strain amplitude [22]. In the future, it would be interesting to perform a detailed comparison of particle dynamics under continuous and cyclic shear.

5 Acknowledgement

This work was supported by NSF-DMR1206351, NSF-DMS1248071, and NASA NNX15AD38G.

References

- [1] M.E. Cates, J.P. Wittmer, J.P. Bouchaud, P. Claudin, Jamming, force chains, and fragile matter, *Phys. Rev. Lett.* **81**, 1841 (1998). [10.1103/PhysRevLett.81.1841](https://doi.org/10.1103/PhysRevLett.81.1841)
- [2] A.J. Liu, S.R. Nagel, The jamming transition and the marginally jammed solid, *Annual Review of Condensed Matter Physics* **1**, 347 (2010). [10.1146/annurev-conmatphys-070909-104045](https://doi.org/10.1146/annurev-conmatphys-070909-104045)
- [3] D. Bi, J. Zhang, B. Chakraborty, R.P. Behringer, Jamming by shear, *Nature* **480**, 355 (2011). [10.1038/nature10667](https://doi.org/10.1038/nature10667)
- [4] E. Brown, H.M. Jaeger, Shear thickening in concentrated suspensions: phenomenology, mechanisms and relations to jamming, *Reports on Progress in Physics* **77**, 046602 (2014). [10.1088/0034-4885/77/4/046602](https://doi.org/10.1088/0034-4885/77/4/046602)
- [5] I.R. Peters, S. Majumdar, H.M. Jaeger, Direct observation of dynamic shear jamming in dense suspensions, *Nature* **532**, 214 (2016). [10.1038/nature17167](https://doi.org/10.1038/nature17167)
- [6] Y. Zhao, H. Hu, Y. Huang, H. Liu, C. Yan, C. Xu, R. Zhang, Y. Wang, Q. Xu, Elasticity-controlled jamming criticality in soft composite solids, *Nature Communications* **15**, 1691 (2024). [10.1038/s41467-024-45964-y](https://doi.org/10.1038/s41467-024-45964-y)
- [7] D. Wang, J. Ren, J.A. Dijksman, H. Zheng, R.P. Behringer, Microscopic origins of shear jamming for 2d frictional grains, *Phys. Rev. Lett.* **120**, 208004 (2018). [10.1103/PhysRevLett.120.208004](https://doi.org/10.1103/PhysRevLett.120.208004)
- [8] R.P. Behringer, B. Chakraborty, The physics of jamming for granular materials: a review, *Reports on Progress in Physics* **82**, 012601 (2018). [10.1088/1361-6633/aadc3c](https://doi.org/10.1088/1361-6633/aadc3c)
- [9] D. Pan, Y. Wang, H. Yoshino, J. Zhang, Y. Jin, A review on shear jamming, *Physics Reports* **1038**, 1 (2023). <https://doi.org/10.1016/j.physrep.2023.10.002>
- [10] A. Abed Zadeh, J. Barés, T.A. Brzinski, K.E. Daniels, J. Dijksman, N. Docquier, H.O. Everitt, J.E. Kollmer, O. Lantsoght, D. Wang et al., Enlightening force chains: a review of photoelasticimetry in granular matter, *Granular Matter* **21**, 83 (2019). [10.1007/s10035-019-0942-2](https://doi.org/10.1007/s10035-019-0942-2)
- [11] D. Howell, R.P. Behringer, C. Veje, Stress fluctuations in a 2d granular couette experiment: A continuous transition, *Phys. Rev. Lett.* **82**, 5241 (1999). [10.1103/PhysRevLett.82.5241](https://doi.org/10.1103/PhysRevLett.82.5241)
- [12] J. Ren, J.A. Dijksman, R.P. Behringer, Reynolds pressure and relaxation in a sheared granular system, *Physical Review Letters* **110**, 018302 (2013). [10.1103/PhysRevLett.110.018302](https://doi.org/10.1103/PhysRevLett.110.018302)
- [13] Y. Zhao, J. Barés, H. Zheng, R.P. Behringer, Tuning strain of granular matter by basal assisted couette shear, *EPJ Web of Conference* **140**, 03049 (2017). [10.1051/epjconf/201714003049](https://doi.org/10.1051/epjconf/201714003049)
- [14] Y. Zhao, J. Barés, H. Zheng, J.E.S. Socolar, R.P. Behringer, Shear-jammed, fragile, and steady states in homogeneously strained granular materials, *Phys. Rev. Lett.* **123**, 158001 (2019). [10.1103/PhysRevLett.123.158001](https://doi.org/10.1103/PhysRevLett.123.158001)
- [15] S. Farhadi, A.Z. Zhu, R.P. Behringer, Stress relaxation for granular materials near jamming under cyclic compression, *Phys. Rev. Lett.* **115**, 188001 (2015). [10.1103/PhysRevLett.115.188001](https://doi.org/10.1103/PhysRevLett.115.188001)
- [16] O. Dauchot, G. Marty, G. Biroli, Dynamical heterogeneity close to the jamming transition in a sheared granular material, *Phys. Rev. Lett.* **95**, 265701 (2005). [10.1103/PhysRevLett.95.265701](https://doi.org/10.1103/PhysRevLett.95.265701)
- [17] H.C. Andersen, Molecular dynamics studies of heterogeneous dynamics and dynamic crossover in supercooled atomic liquids, *Proceedings of the National Academy of Sciences* **102**, 6686 (2005). [10.1073/pnas.0500946102](https://doi.org/10.1073/pnas.0500946102)
- [18] C. Toninelli, M. Wyart, L. Berthier, G. Biroli, J.P. Bouchaud, Dynamical susceptibility of glass formers: Contrasting the predictions of theoretical scenarios, *Phys. Rev. E* **71**, 041505 (2005). [10.1103/PhysRevE.71.041505](https://doi.org/10.1103/PhysRevE.71.041505)
- [19] N. Lačević, F.W. Starr, T.B. Schröder, S.C. Glotzer, Spatially heterogeneous dynamics investigated via a time-dependent four-point density correlation function, *The Journal of Chemical Physics* **119**, 7372 (2003). [10.1063/1.1605094](https://doi.org/10.1063/1.1605094)
- [20] C. Coulais, R.P. Behringer, O. Dauchot, How the ideal jamming point illuminates the world of granular media, *Soft Matter* **10**, 1519 (2014). [10.1039/C3SM51231B](https://doi.org/10.1039/C3SM51231B)
- [21] B. Kou, Y. Cao, J. Li, C. Xia, Z. Li, H. Dong, A. Zhang, J. Zhang, W. Kob, Y. Wang, Translational and rotational dynamical heterogeneities in granular systems, *Phys. Rev. Lett.* **121**, 018002 (2018). [10.1103/PhysRevLett.121.018002](https://doi.org/10.1103/PhysRevLett.121.018002)
- [22] Y. Zhao, Y. Zhao, D. Wang, H. Zheng, B. Chakraborty, J.E.S. Socolar, Ultrastable shear-jammed granular material, *Phys. Rev. X* **12**, 031021 (2022). [10.1103/PhysRevX.12.031021](https://doi.org/10.1103/PhysRevX.12.031021)